ACS NANO

www.acsnano.org

ARTICLE

Interfacial Chemistry Modulation via Amphoteric Glycine for a Highly Reversible Zinc Anode

Yu Liu, Yongkang An, Lu Wu, Jianguo Sun, Fangyu Xiong, Han Tang, Shulin Chen, Yue Guo, Lei Zhang, Qinyou An,* and Liqiang Mai*

Cite This: *ACS Nano* 2023, 17, 552–560

Read Online

ACCESS | Metrics & More | Article Recommendations | Supporting Information

ABSTRACT: **Zn metal is thermodynamically unstable in aqueous electrolytes, which induces dendrite growth and ongoing parasitic reactions at the interface during the plating process and even during shelf time, resulting in rapid battery failure and hindering the practical application of aqueous Zn ion batteries. In this work, glycine, a common multifunctional additive, is utilized to modulate the solvation shell structure and enhance the interfacial stability to guard the reversibility and stability of the Zn anode. Apart from partially replacing the original SO_4^{2-} in the contact ion pair of $Zn^{2+}[H_2O]_5{\cdot}OSO_3^{2-}$ complexes to suppress the formation of $Zn_4(OH)_6SO_4{\cdot}xH_2O$ byproducts at the interface, glycine molecules can also form a water-poor electrical double layer on the zinc metal surface during resting and be further reduced to build *in situ* a ZnS-rich solid electrolyte interphase (SEI) layer during cycling, which further suppresses side reactions and the random growth of Zn dendrites in the whole process. As expected, the cycle life of the symmetrical cells reaches over 3200 h in glycine-containing electrolytes. In addition, the Zn//NVO full cell shows exceptional cycling stability for 3000 cycles at 5 A g^{-1}. Given the low-cost superiority of glycine, the proposed strategy for interfacial chemistry modulation shows considerable potential in promoting the commercialization progress of aqueous batteries.**

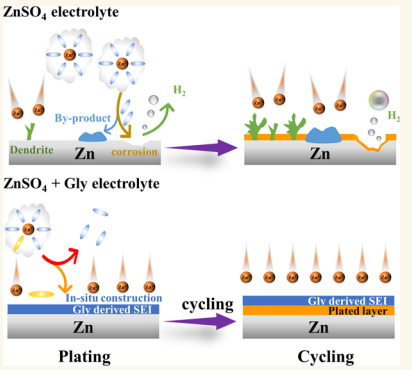

KEYWORDS: *glycine, solvation structure, solid electrolyte interphase chemistry, Zn metal anode, Zn ion batteries*

1. INTRODUCTION

Among the promising candidates for large-scale energy storage beyond Li ion batteries, aqueous Zn metal batteries (AZMBs) have attracted widespread attention due to their inherently high safety and low cost.[1−5] Furthermore, a Zn anode also provides a high specific capacity (820 mAh g^{-1}, 5855 mAh cm^{-3}) and an appropriate electrochemical potential (−0.76 V vs normal hydrogen electrode (NHE)).[6−9] However, the practical application of AZMBs still faces inevitable hurdles because of the poor reversibility of the Zn anode caused by the unstable electrolyte−anode interface.[10−12] During battery resting or operation, active water molecules will attack the zinc metal and trigger parasitic side reactions, bringing on a more uneven zinc surface that might lead to a decreased plating/stripping reversibilty, the formation of zinc dendrites, and serious battery deterioration.[13−15]

To improve the stability of the Zn anode, it is significantly important to suppress the reactivity of water in the electrolyte and increase the stability of the zinc anode interface. Previously, some functional materials including montmorillonite, nano-$CaCO_3$, and P(VDF-TrFE) were reported as coatings on a Zn anode to regulate uniform Zn^{2+} flux, thus suppressing the dendrite growth.[16−18] However, the traditional *ex situ* artificial protective layers not only increase the interfacial resistance and lower the diffusion kinetics of Zn^{2+} but are also easily pulverized during continuous plating/stripping. In contrast, *in situ* construction of protective layers on a Zn anode has been demonstrated to be more efficient. For example, Zhang et al. reported that the *in situ* formation of a ZnTA (tannin acid)-derived anticorrosive layer can suppress the parasitic reactions and improve the reversibility of Zn^{2+} plating/stripping.[19] Similar anticorrosive films such as a phytic acid film,[20] cerium-based films, etc.[21] have also been investigated to possess comparable effectiveness. Regrettably, such a protective-layer-based chemical transformation methods

Received: September 19, 2022
Accepted: December 9, 2022
Published: December 16, 2022

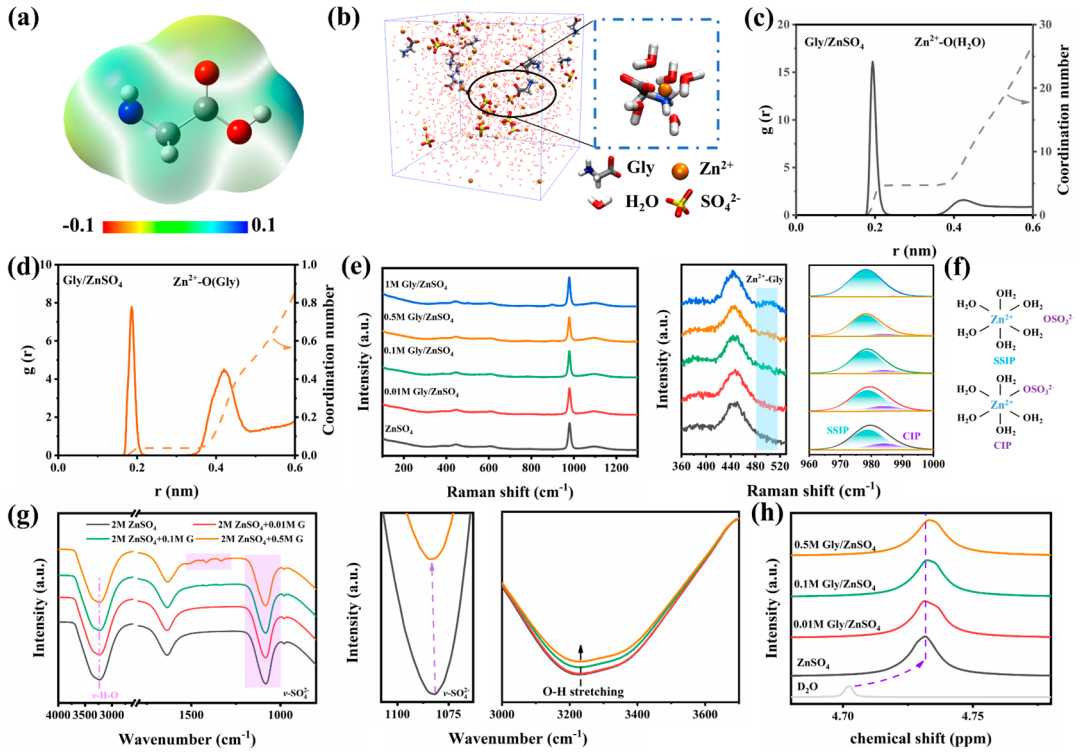

Figure 1. (a) Electrostatic potential mapping of a Gly molecule. MD simulations of Gly/$ZnSO_4$ electrolyte: (b) 3D snapshot and (c, d) corresponding $g(r)$ and $N(r)$ results. (e) Raman spectra for 2 M $ZnSO_4$ without and with various concentrations of Gly. (f) Two Zn^{2+} solvation structures in Gly/$ZnSO_4$ electrolyte. (g) FT-IR spectra and (h) ^2H NMR spectra for 2 M $ZnSO_4$ without and with various concentrations of Gly.

are prone to failure after long cycling, especially at high current density, because of the poor physical interaction with the Zn subtrate. Even though in our previous work we found that a low-cost glutamate (Glu^-) additive can well stabilize the zinc anode by forming an organic SEI layer composed of Glu^- reduction products, the unsatisfactory Zn^{2+} diffusion ability across the SEI layer is still a non-negligible threat because of the lack of movable Zn^{2+} in the Glu^--decomposition-derived simple SEI.[22] Different from the additive's decomposition-derived SEI, manipulating interfacial chemistry to construct a robust chemical-bonding-anchored SEI layer seems to be more attractive. Together with regulating the Zn^{2+} solvation shell structure, an active SEI with feasibly fast Zn^{2+} diffusion ability can be further obtained.[23,24] However, how to design a unique species that can synergistically optimize the ion solvation shell structure and interfacial reactions is still a mystery.

Herein, Gly is investigated as a low-cost electrolyte additive for AZMBs. Combining experimental analysis, molecular dynamics (MD) simulations, and DFT calculations, it is demonstrated that Gly can not only regulate the surface absorption environment of Zn anode but also modulate the primary solvation shell of Zn^{2+}, which can alleviate the uncontrollable growth of dendrites and byproducts. Most importantly, the Gly adsorbed on the zinc surface has a lower LUMO level and undergoes a reduction reaction prior to Zn^{2+} to *in situ* construct a ZnS-rich SEI layer during cycling, which has been definitively verified by XPS and TEM characterization. By separating Zn anodes from free water molecules, this Gly-derived SEI protective layer could further stifle unwanted side reactions and improve Zn reversibility. As expected, the Zn||Zn symmetrical cell and Zn||$NH_4V_4O_{10}$ full cell using a Gly-containing electrolyte display cycling stability (3200 h and 3000 cycles) superior to that in a bare $ZnSO_4$ electrolyte. This strategy of *in situ* construction of an SEI via the reduction of additives with low LUMO energy at the Zn anode interface provides a promising direction for future interfacial modulation in aqueous battery chemistry.

2. RESULTS AND DISCUSSION

Similar to its wide application in the electroplating process, glycine (Gly), the smallest amino acid, can also be employed in electrolytes because both carboxyl and amino functional groups in the small molecules can chelate with metal ions, thus manipulating the solvation shell structure of metal ion−H_2O complexes. As shown in the electrostatic potential mapping of a Gly molecule (Figure 1a), it is obvious that the amino and carbonyl groups in the Gly molecule have a negative electrostatic potential, implying that electrostatic attraction between Zn^{2+} and the Gly molecule can be enhanced. As shown in Figure 1b, vivid MD simulations for the Gly/$ZnSO_4$ electrolyte were performed. A new solvation shell structure of Zn^{2+} composed of five H_2O and one Gly molecule was observed in a uniformly distributed Gly/$ZnSO_4$ system, which indicates that Gly will chelate with zinc ions and break the primary solvation shell structure (PSS). Detailed statistical results of radial distribution functions (RDFs) for Zn−O from both H_2O and Gly are exhibited in Figure 1c,d. They clearly show that a characteristic peak emerged at around 0.2 nm in Zn^{2+}−O (Gly), in line with the position of the original H_2O in Zn^{2+}−O (H_2O). The average coordination numbers of Zn^{2+}−O (H_2O) and Zn^{2+}−O (Gly) in the first-hydration-layer Gly/$ZnSO_4$ electrolytes are around 4.6 and 0.05, respectively. These suggest that Gly molecules can enter the solvation shell structure and remain stable. To better

https://doi.org/10.1021/acsnano.2c09317
ACS Nano 2023, 17, 552−560

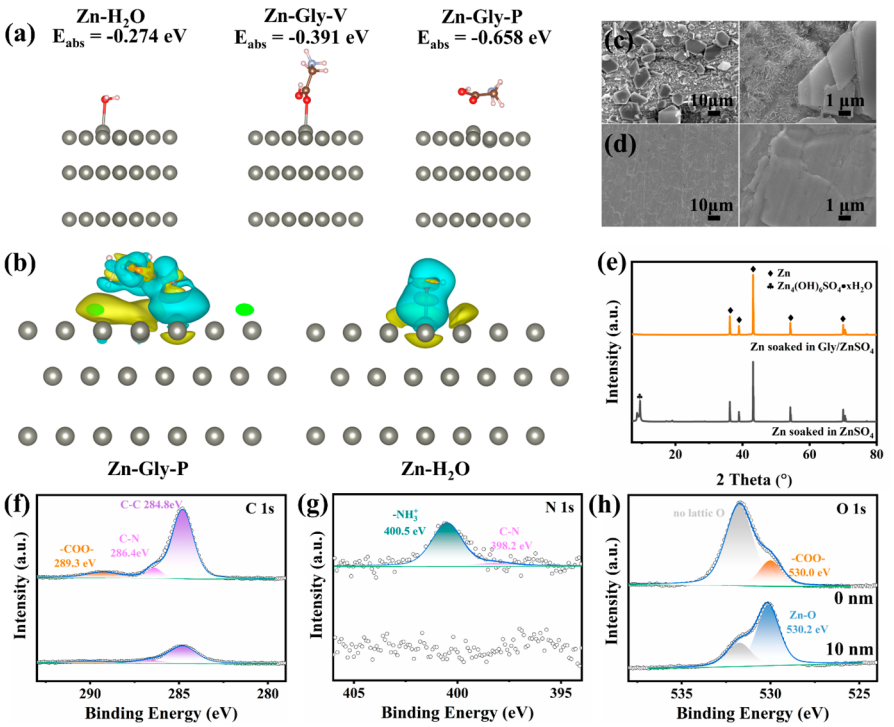

Figure 2. (a) Absorption energy comparison of H_2O and Gly molecules on a Zn (002) surface and corresponding absorption models. (b) Charge density difference of the Zn (002) surface with Gly molecules and H_2O adsorption. SEM images of the Zn soaked in (c) $ZnSO_4$ and (d) Gly/$ZnSO_4$ for 5 days. (e) XRD patterns of the Zn soaked in $ZnSO_4$ and Gly/$ZnSO_4$ for 5 days. High-resolution XPS depth spectra of Zn anode soaked in Gly: (f) C 1s, (g) N 1s, and (h) O 1s.

understand the interaction of Gly additives with various constituents in the initial $ZnSO_4$ electrolyte, Raman, FT-IR, and nuclear magnetic resonance (NMR) were used. As displayed in Figure 1e, a new peak that emerged near 490 cm^{-1} can be assigned to the chelation of Gly and a Zn ion when the content of Gly increases to 1 M, which is in line with MD simulation results. Furthermore, another peak that emerged near 980 cm^{-1} can be assigned to the ν-SO_4^{2-} band. Based on the classic Eigen−Tamm (ET) mechanism, such strong peaks can be deconvoluted into two ion pairs of the contact ion pair (CIP) and the solvent-separated ion pair (SSIP) (Figure 1f), respectively.[25−27] As the concentration of Gly increases, the peak of the ν-SO_4^{2-} band shifts to a lower frequency and the proportion of CIPs gradually decreases compared to 24.9% in the $ZnSO_4$ electrolyte, suggesting that the Gly molecule can easily enter the CIP and replace one of the original SO_4^{2-} groups, which is beneficial to suppress the formation of $Zn_4(OH)_6SO_4{\cdot}xH_2O$ byproducts.[28]

The weakening effect of Gly on the interaction between Zn^{2+} and SO_4^{2-} was further confirmed through FT-IR results (Figure 1g). In addition to the characteristic vibration peaks from Gly molecules (1332, 1415, 1450, and 1512 cm^{-1}),[29] a blue shift of the stretching vibration of ν-SO_4^{2-} (1081.1 cm^{-1} for bare $ZnSO_4$ electrolyte and 1084.6 cm^{-1} for 2 M $ZnSO_4$ + 0.5 M Gly) appears after the introduction of Gly additives, suggesting the electrostatic coupling between Zn^{2+} and SO_4^{2-} has been broken, which further demonstrates that a CIP solvation structure has been suppressed.[30] Furthermore, another obvious broad peak appearing at 3000−3700 cm^{-1} can be attributed to the OH-stretching vibration of water. It can be further deconvoluted into three components of strong H-bonds (~3230 cm^{-1}), weak H-bonds (~3450 cm^{-1}), and non H-bonds (~3620 cm^{-1}).[31] For the bare $ZnSO_4$ electrolyte, the strong H-bonds account for the highest proportion in the H-bond environment. However, the intensity of strong H-bond decreases more quicly than that of other H-bonds upon thean increase in concentration of Gly, implying that the proportion of strong H-bonds is reduced and the water activity is suppressed.[32] More solid evidence can be found in the NMR spectra (Figure 1h), which exhibits that the ^2H peak shifts to 4.731 ppm compared to 4.702 ppm for bare D_2O after the introduction of $ZnSO_4$, which should be ascribed to a decrease of free water molecules due to the strong coordination between Zn^{2+} and D_2O. Such a peak further shifts to 4.733 ppm after the subsequent introduction of Gly (0.5 M), implying free water molecules are further decreased. This once again proves that Gly interacted strongly with H_2O and the hydrogen bond networks among H_2O molecules were restructured, which further certified the suppressed hydrogen evolution reaction.[28,32]

To understand the working mechanism of the Gly additives at the Zn anode interface, *ab initio* DFT calculations and surface chemistry and micromorphological experiments were performed. Figure 2a displays the absorption energies of Gly and H_2O at various possible positions on a Zn (002) facet. Due to the strong interaction induced by more charge transfer between the carboxyl group of Gly and the bare Zn atoms (Figure 2b), the adsorption energy of Gly with parallel absorption on the Zn (Zn-Gly-P, −0.658 eV) is lower than that of Gly with vertical absorption on the Zn (Zn-Gly-V, −0.391 eV) and Zn−H_2O (−0.274 eV), implying that the electrical double layer (EDL) structure of the Zn surface is mainly composed of Zn-Gly-P.[33] Constrained by current computing resources, the adsorption energy results are obtained from an ideal and general simulation method to verify that the introduction of Gly will preferentially adsorb on the zinc

https://doi.org/10.1021/acsnano.2c09317
ACS Nano 2023, 17, 552−560

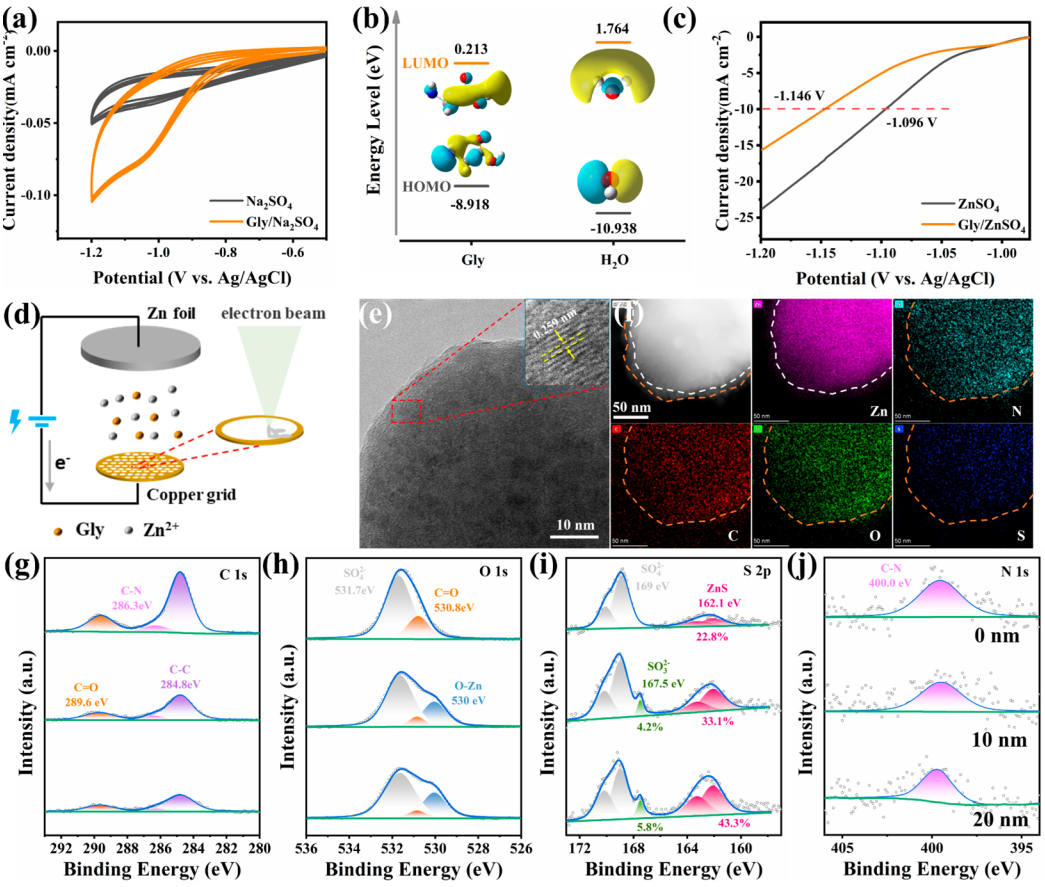

Figure 3. (a) CV curves of Na_2SO_4 and Gly/Na_2SO_4 electrolyte at 10 mV s^{-1}. (b) HOMO−LUMO energy levels of Gly and water molecules. (c) Comparison of HER performance in $ZnSO_4$ and Gly/$ZnSO_4$ electrolyte systems. (d) Schematic diagram of plated Zn on a copper grid using Gly/$ZnSO_4$ electrolyte at 4 mA cm^{-2} to prepare a TEM sample. (e) TEM image and (f) HAADF image and corresponding elemental mapping of the sample. High-resolution XPS depth spectra of Zn anode cycled in Gly/$ZnSO_4$ electrolyte for 20 cycles: (g) C 1s, (h) O 1s, (i) S 2p, and (j) N 1s.

surface and inhibit side reactions, without consideration of the effects of salt and solvent in the actual situation. Control experiments of soaking an Zn anode in $ZnSO_4$ electrolyte with or without Gly were further performed to examine the practical impact of the EDL structure on the Zn surface. Compared with bare $ZnSO_4$ electrolyte, the surface of Zn metal soaked in Gly/$ZnSO_4$ electrolyte for 5 days is more uniform and smooth, and no obvious byproducts can be observed (Figure 2c,d), suggesting that the absorbed Gly layer can effectively block the side reactions of Zn in $ZnSO_4$ electrolyte, as confirmed by XRD (Figure 2e and Figure S4). Afterward, X-ray photoelectron spectroscopy (XPS) was applied to investigate the binding structure between absorbed Gly and the Zn anode (Figure S5 and Figure 2f,g). For the pure Gly, due to the zwitterionic structure of Gly in the solid state, characteristic peaks of protonated amino groups (NH_3^+) and deprotonated carboxyl groups (COO^-) can be observed from N 1s and O 1s spectra (Figure S6).[34] For the Zn metal after being soaked in Gly/$ZnSO_4$, apparent peaks of C−N and strong amino groups appear in C 1s (Figure 2f) and N 1s spectra (Figure 2g). Additionally, compared to the peak of carboxyl groups of Gly in O 1s spectra, the peak of COO-Zn becomes broadened and shifts to lower binding energy (Figure 2h), indicating that Gly chemically absorbs on the Zn surface instead of weakly physically absorbs. Such a strong chemical adsorption introduces a water-poor EDL, which can effectively inhibit the competitive adsorption of H_2O and its subsequent induced side reactions.[33]

As it was demonstrated above that Gly has a lower adsorption energy and can more easily form an EDL at the electrode−electrolyte interface, how the EDL evolves during the Zn plating process is still the main concern, especially in light of its effects on the diffusion kinetics of Zn^{2+} and the thermodynamic stability of the Zn anode. Figure 3a shows CV curves of Gly/Na_2SO_4 and Na_2SO_4 electrolytes. The reduction current density in the Gly/Na_2SO_4 electrolyte started to rise in comparison to that in the control electrolyte at −0.95 V (vs Ag/AgCl), which is prior to the standard potential of Zn deposition (−0.984 V vs Ag/AgCl), and doubled at −1.20 V (vs Ag/AgCl). In contrast, little change in the oxidation current density can be observed, indicating that Gly will be reduced preferentially to Zn^{2+} on the Zn anode surface to form a stable SEI layer. Besides, this proves that Gly exhibits a higher highest occupied molecular orbital (HOMO) and lower lowest unoccupied molecular orbital (LUMO) than those of H_2O (−8.918 vs −10.938 eV, 0.213 vs 1.764 eV) (Figure 3b), implying that Gly can easily obtain electrons and will be reduced to the SEI ahead of H_2O, thus suppressing the side reaction on the Zn surface and therefore producing fewer byproducts. To accurately prove the reliable formation of the SEI by the reduction of absorbed Gly, we did not use the traditional focused ion beam (FIB) process to prepare

https://doi.org/10.1021/acsnano.2c09317
ACS Nano 2023, 17, 552−560

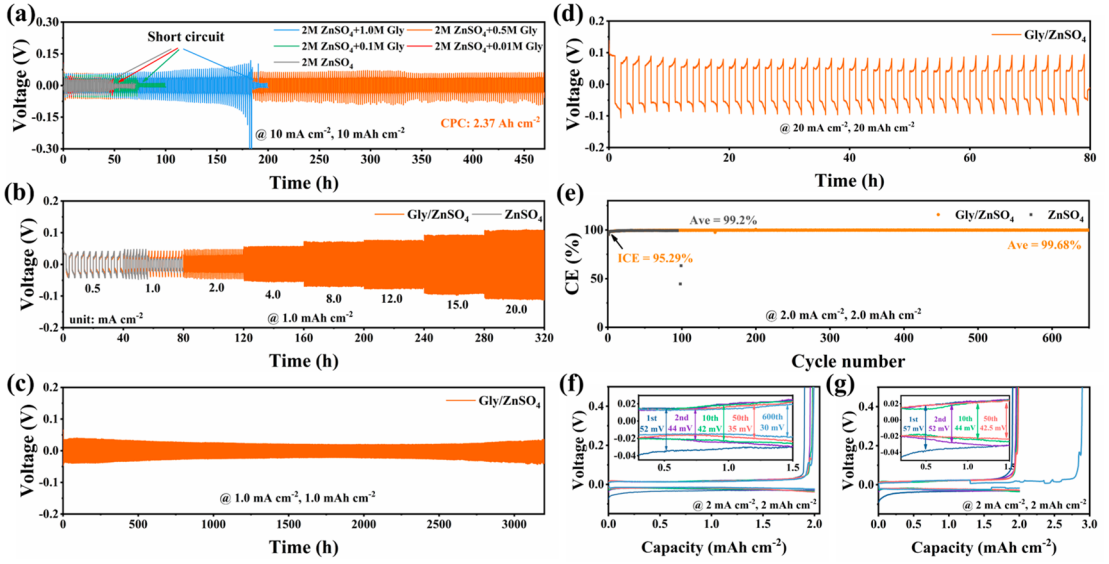

Figure 4. (a) Voltage−time curves of Zn||Zn symmetrical cells using $ZnSO_4$ electrolyte with various concentrations of Gly at 10 mA cm^{-2} and 10 mAh cm^{-2}. (b) Rate capability of Zn||Zn symmetrical cells using different electrolytes. Voltage−time curves of a Zn||Zn symmetrical cell using Gly/$ZnSO_4$ electrolyte at (c) 1 mA cm^{-2} and 1 mAh cm^{-2} and(d) 20 mA cm^{-2} and 20 mAh cm^{-2}. (e) Coulombic efficiency of Zn||Cu cells using different electrolytes at 2 mA cm^{-2} and 2 mAh cm^{-2} and corresponding voltage profiles at various cycles in (f) Gly/$ZnSO_4$ and (g) $ZnSO_4$ electrolyte.

transmission electron microscopy (TEM) samples from Zn metal anode because of the destruction from ion beam bombardment. Instead, we directly deposited Zn on a blank TEM copper grid using the Gly/$ZnSO_4$ electrolyte by the same process as in our electrochemical testing to obtain better accuracy, and carried out a TEM characterization (Figure 3d). As shown in Figure 3e, clear lattice fringes corresponding to the (002) lattice plane of Zn are observed in the TEM image, indicating that Zn particles have been successfully deposited on the copper grid. Impressively, ultrathin amorphous layers are observed on the outer layer of the Zn particles from the high-angle annular dark-field (HAADF) image (Figure 3f). In the energy dispersive X-ray spectroscopy (EDS) mapping, it can be observed that the Zn element is mainly concentrated in the center of the particle (in the white dotted line) and a trace is also distributed evenly on the particle's outer layer (between the white dotted line and the yellow dotted line), while N, C, O, S elements are uniformly dispersed on the whole particle surface (in the orange dotted line), indicating that such an ultrathin amorphous SEI layer is composed of zinc salts and *in situ* Gly reduction products during the zinc plating process (Figure 3f). Moreover, XPS spectra were measured to analyze the possible composition of the *in situ* formed SEI. The intensities of C−N and C═O peaks obviously tended to stabilize after an increase in the sputtering depth (Figure 3g,h,j). Besides, the characteristic peak of amine (at 399.7 eV) can be observed stably at different depths of N 1s XPS spectra (Figure 3j), indicating that Gly or its derivatives are homogeneously present in the SEI layer. Furthermore, the signal of sulfate can also be observed in the O 1s spectra (Figure 3h), which may be attributed to the precipitation of zinc salts in the electrolyte.[14] More interestingly, the high-resolution S 2p spectra not only confirm the existence of SO_4^{2-} (169.0 eV, 77.2%) but also imply the existence of ZnS species (162.1 eV, 22.8%) (Figure 3i).[33,35] Simultaneously, with an increase in the sputtering depth, the SO_4^{2-} content decreased to 50.9%, the ZnS species content increased to 43.3%, and minor SO_3^{2-} species (167.5 eV, 5.8%) appeared, suggesting the formation of a ZnS-rich solid electrolyte interphase, which is in line with the EDS results.[33] For Zn metal deposited in bare $ZnSO_4$ electrolyte, only the characteristic peak of SO_4^{2-} is observed in the S 2p spectra (Figure S8b), indicating that the SO_3^{2-} and ZnS components may originate from the reduction of SO_4^{2-} by H_2 generated from the electrochemical reaction between Gly and Zn during the initial cycles.[35] According to previous reports, ZnS plays an important role in improving the stability and reversibility of Zn anodes.[36,37]

To fully understand the positive effect of the *in situ* constructed SEI on stabilizing the Zn anode and regulating the deposition behavior, the structure and morphology of the deposited Zn and the electrochemical properties of both $ZnSO_4$ and Gly/$ZnSO_4$ electrolytes were further investigated. As shown in Figure 3c and Figure S9, the Zn anode in Gly/$ZnSO_4$ electrolyte possesses a lower corrosion current density (from 0.56 to 0.1 mA cm^{-2}) and a broader HER potential (from −1.096 to −1.146 V) than that in $ZnSO_4$ electrolyte, which is in line with adsorption energy results. This indicates that the corrosion and HER reactions have been effectively suppressed by the *in situ* SEI in Gly/$ZnSO_4$ electrolyte. Figure S10 shows the chronoamperometry curves of the Zn tested in the three-electrode system using $ZnSO_4$ and Gly/$ZnSO_4$ electrolytes at an overpotential of −150 mV (vs Ag/AgCl). During the whole plating process up to 500 s, the current response at the Zn anode in Gly/$ZnSO_4$ electrolyte quickly reaches the equilibrium state and eventually maintains a smaller constant value than that in $ZnSO_4$ electrolyte. This implies that the *in situ* SEI layer effectively restricts the intractable two-dimensional diffusion of Zn^{2+} during the plating process, thus promoting the uniformity of plated Zn and suppressing Zn dendrite growth. In addition, the Zn^{2+} diffusion kinetic behavior in the SEI layer was also evaluated by the activation energies of Zn||Zn symmetrical batteries after 20 cycles (Figure S11). It is evident that the Zn anode in Gly-containing electrolyte possesses a lower active energy (29.4 kJ

https://doi.org/10.1021/acsnano.2c09317
ACS Nano 2023, 17, 552−560

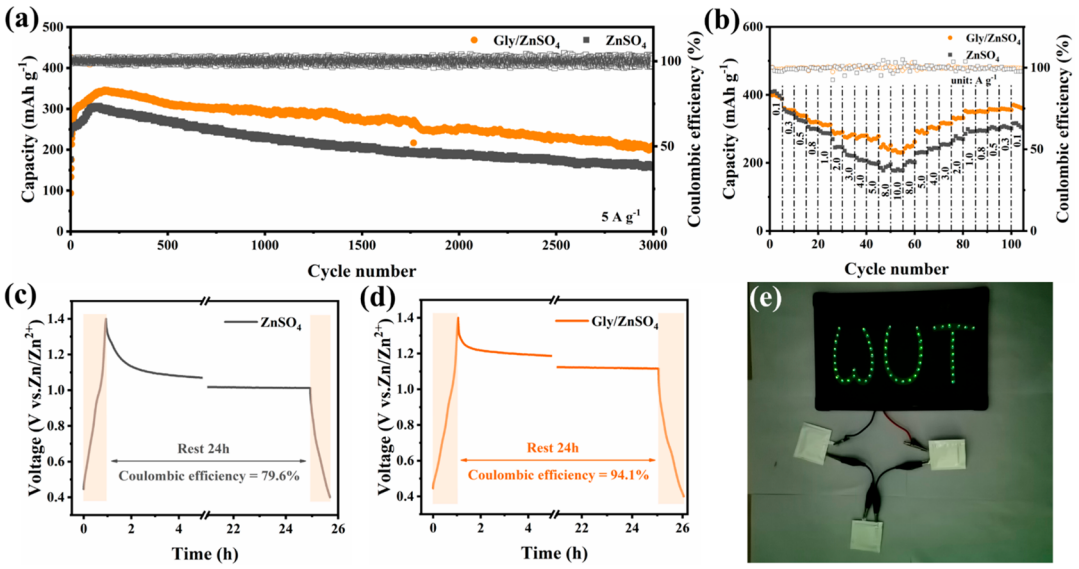

Figure 5. (a) Cycling performance at 5 A g^{-1} and (b) rate capability of Zn||NVO cells in different electrolytes. Self-discharge test of the Zn||NVO cells using (c) $ZnSO_4$ and (d) Gly/$ZnSO_4$ electrolytes. (e) LEDs lighted by the Zn||NVO pouch cells in Gly/$ZnSO_4$ electrolytes.

mol^{-1}) compared to that in the blank electrolyte (36.8 kJ mol^{-1}), indicating fast desolvation of Zn^{2+} can be achieved after the *in situ* construction of a Gly-derived SEI on the Zn surface.[38,39] Moreover, it is worth noting that Zn anodes using Gly/$ZnSO_4$ electrolyte show a flatter and denser deposited layer and no byproducts appear compared to those using blank electrolyte after cycling (Figures S12 and S13).

To further investigate the effect of Gly additive on the stability and reversibility of the zinc ion battery, Zn||Zn symmetrical cells and Zn||Cu asymmetrical cells were assembled and tested after obtaining the optimized Gly concentration of 0.5 M (Figure 4a). As displayed in Figure 4a, the symmetrical cell using Gly/$ZnSO_4$ electrolyte delivered stable cycling for 460 h corresponding to a cumulative plated capacity of 2.37 Ah cm^{-2} and a low overpotential at 10 mA cm^{-2} and 10 mAh cm^{-2}, while the symmetrical cell using blank electrolyte quickly short-circuited after only 48 h of cycling. As shown in Figure 4b, symmetrical cells quickly show a voltage dip and a short circuit in the bare $ZnSO_4$ electrolyte. In contrast, the symmetrical batteries using Gly/$ZnSO_4$ electrolyte show a stable and flat voltage profile and a small voltage hysteresis even at various current densities. Such excellent stability can be mainly attributed to the improved Zn^{2+} transport kinetics by the Gly-derived SEI. Long cycling testing of the Zn||Zn symmetrical batteries was further applied to investigate the ability to inhibit dendrite formation/growth under competitive test conditions. Compared to the blank electrolyte, the symmetrical batteries using Gly/$ZnSO_4$ electrolyte exhibit better cycling stability. More attractively, symmetrical batteries using Gly/$ZnSO_4$ electrolyte displayed a superlong cycle life of 3200 h at 1 mA cm^{-2} and 1 mAh cm^{-2}. Even at 20 mA cm^{-2} and 20 mAh cm^{-2}, the symmetrical cell is stably cycled for 80 h with a low voltage hysteresis (<0.2 V), which is much better than those in most previous works[28,38,40−45] (Figure 4c,d). Subsequently, the Zn reversibility behavior was investigated in Zn||Cu asymmetrical cells at 2 mA cm^{-2} and 2 mAh cm^{-2} (Figure 4e−g). The asymmetrical cell using Gly/$ZnSO_4$ electrolyte shows a higher initial Coulombic efficiency (ICE) of 95.29% and can run for over 650 cycles with a high average CE (ACE) of 99.68%, much higher than that in the blank electrolyte (ACE of 99.2% for 90 cycles). Excitingly, even under the condition of 5 mA cm^{-2} and 5 mAh cm^{-2} (beyond practical conditions of 4 mA cm^{-2} and 4 mAh cm^{-2}), the asymmetrical cell still exhibits an ultrahigh ICE of 96.71% and ACE of 99.7% over 110 cycles (Figure S14), indicating that the cycling stability and reversibility of the batteries were both improved after *in situ* construction of the Gly-derived SEI. To verify whether the Gly additive possesses a similar effect in electrolytes with other Zn salts, symmetrical cells using $Zn(CF_3SO_3)_2$ electrolyte with or without Gly additive were explored. As shown in Figure S15, the symmetrical cells using Gly/$Zn(CF_3SO_3)_2$ electrolyte exhibit better cycling stability than that in bare $Zn(CF_3SO_3)_2$ electrolyte, indicating that the Gly additive has a similar effect in aqueous electrolytes containing different Zn salts.

Subsequently, Zn-based full cells based on ammonium vanadium oxide ($NH_4V_4O_{10}$, NVO) cathodes were performed to explore the practical application potential of the Gly-modified electrolyte. During the initial cycles, the capacities of full cells using $ZnSO_4$ without and with Gly show a similar transitory increasing behavior due to the activation process of NVO at 5 A g^{-1} (Figure 5a). However, the cell using the Gly-containing electrolyte shows excellent stability and maintains a higher specific capacity of 211.4 mAh g^{-1} after 3000 cycles with a high CE of 99.55% (~1.32-fold of that in the blank electrolyte). It is more notable that the rate capability of the Zn||NVO full cell using Gly/$ZnSO_4$ electrolyte exhibits superior performance compared to that using $ZnSO_4$ electrolyte (Figure 5b). Specifically, in the Gly/$ZnSO_4$ electrolyte, the full cell delivers a high discharge capacity of 400 mAh g^{-1} with a high CE of 99.15% at 0.1 A g^{-1} and 57.8% capacity retention at 10 A g^{-1}. Moreover, when the current was gradually returned to 0.1 A g^{-1}, the cell still delivered a reversible specific capacity of 365 mAh g^{-1}, exhibiting a high capacity retention rate of up to 91.2%. In contrast, for the bare $ZnSO_4$ electrolyte, the cell only delivers lower rate capacities and a lower capacity retention (43.8%) when the current density increases from 0.1 A g^{-1} to 10 A g^{-1}. When the current returned to 0.1 A g^{-1}, the cell delivered a plummeting reversible specific capacity of 311 mAh g^{-1}, exhibiting a lower capacity retention rate of only

https://doi.org/10.1021/acsnano.2c09317
ACS Nano 2023, 17, 552−560

76.9%. Impressively, the full cells using Gly/$ZnSO_4$ electrolytes also show a lower overpotential even at higher current density, as presented in the galvanostatic charge/discharge (GCD) profiles in Figure S18. In addition, Figure 5c,d shows the self-discharging test of full cells using $ZnSO_4$ or Gly/$ZnSO_4$ electrolyte. To reduce the artificial error, the Zn||NVO cells were activated for 15 cycles at 0.3 A g^{-1} before the self-discharge test. The Zn||NVO cell using Gly-containing electrolyte shows a CE of 96.1%, higher than that of 79.6% in the blank electrolyte. The greatly improved electrochemical performance could be attributed to the comprehensive effect of the Gly-derived SEI in inhibiting the unwanted side reaction and dendrite growth at the Zn anode side, together with the promotion of zinc ion diffusion kinetics. Furthermore, three series-connected pouch cells using Gly/$ZnSO_4$ electrolyte can light 55 light-emitting diodes (LEDs) (Figure 5e), demonstrating the commercial potential of Gly-containing electrolyte in AZIBs.

3. CONCLUSIONS

In this work, Gly is used as an electrolyte additive to construct an *in situ* SEI layer on a Zn anode to stabilize ZMBs. The Gly additive can suppress side reactions and regulate the uniform deposition of Zn^{2+} during standing or even cycling through the following mechanisms. (1) The additive can manipulate the solvation shell structure of Zn^{2+} and HBNs and thus prevent side reactions at the interface. (2) The additive can more easily aggregate on the Zn surface in comparison to water to form an EDL structure, which directly isolates the contact between water and the Zn anode during relaxation. (3) The additive can undergo a reduction reaction prior to the reduction of Zn^{2+} to form an *in situ* ZnS-rich SEI to improve the Zn^{2+} desolvation and plating/stripping kinetics. As a result, the Zn||Zn cells using Gly/$ZnSO_4$ electrolyte exhibit a stable cyclability of 3200 h at 1 mA cm^{-2} and 1 mAh cm^{-2} and of 460 h at 10 mA cm^{-2} and 10 mA cm^{-2}. Impressively, the Zn||Cu cells using Gly/$ZnSO_4$ electrolyte show a higher ICE of 95.29% and can run over 650 cycles with a higher ACE of 99.68%, much more than those of blank electrolyte and previous reports. Moreover, the Zn||NVO full cell using a Gly-containing electrolyte exhibit a higher capacity (231.3 mAh g^{-1} at 10 A g^{-1}) and markedly enhanced cycling stability (211.4 mAh g^{-1} after 3000 cycles with a high CE of 99.55%) than those in the bare blank electrolyte, demonstrating the significant impact of glycine in improving the performance for ZIBs.

4. METHODS

4.1. Electrolyte Preparation. Zn foil (>99.99%, 100 μm) was purchased from SCI Materials Hub, and Cu foil (>99.99%, 50 μm) was obtained from Tengfeng metal. $Zn(CF_3SO_3)_2$ (98%), $ZnSO_4 \cdot 7H_2O$ (99%), glycine (Gly, 99%), and $NaSO_4$ (99%) were purchased from Aladdin. The electrolytes were prepared by adding a 2 M $ZnSO_4 \cdot 7H_2O$ salt and different concentrations of Gly (0, 0.01, 0.1, 0.5, and 1 M) into deionized water. The optimized concentration of Gly is 0.5 mol L^{-1}, denoted Gly/$ZnSO_4$. $Zn(CF_3SO_3)_2$-based electrolytes were prepared by a similar method. Two solutions (0.5 M Na_2SO_4 without and with 0.1 M Gly) were prepared to determine the decomposition potential of Gly.

4.2. Synthesis of Ammonium Vanadium Oxide ($NH_4V_4O_{10}$, *NVO*). First, 2.0 g of yellow V_2O_5 was added to 10 mL of NH_4OH (30%), and the mixture turned brown after stirring. Then, this mixture was added to 70 mL of an oxalic acid solution ($C_2H_2O_4$, 0.1 M) and continuously stirred. After 30 min, hydrochloric acid (HCl, 37%) was added dropwise to the solution until its pH reached around 3. The solution was then heated at 190 °C for 5 h. Finally, the $NH_4V_4O_{10}$ was washed and then vacuum-dried overnight.

The $NH_4V_4O_{10}$ electrode was made from a mixture of active material (70%), 20% Ketjen Black (20%), and polytetrafluoroethylene (PTFE) binder (10%). Then, the mixture was uniformly dispersed in isopropanol solvent and rolled repeatedly until forming a film, and then the film was vacuum-dried for 12 h and transferred to a titanium mesh for use.

ASSOCIATED CONTENT

Supporting Information

The Supporting Information is available free of charge at https://pubs.acs.org/doi/10.1021/acsnano.2c09317.

Experimental procedures, including materials characterization, electrochemical measurements, MD simulations, and DFT calculation methods, additional materials characterization, and electrochemical data (PDF)

AUTHOR INFORMATION

Corresponding Authors

Qinyou An − *State Key Laboratory of Advanced Technology for Materials Synthesis and Processing, Wuhan University of Technology, Wuhan 430070, People's Republic of China; Foshan Xianhu Laboratory of the Advanced Energy Science and Technology Guangdong Laboratory, Foshan 528200, People's Republic of China;* orcid.org/0000-0003-0605-4942; Email: anqinyou86@whut.edu.cn

Liqiang Mai − *State Key Laboratory of Advanced Technology for Materials Synthesis and Processing, Wuhan University of Technology, Wuhan 430070, People's Republic of China; Foshan Xianhu Laboratory of the Advanced Energy Science and Technology Guangdong Laboratory, Foshan 528200, People's Republic of China;* orcid.org/0000-0003-4259-7725; Email: mlq518@whut.edu.cn

Authors

Yu Liu − *State Key Laboratory of Advanced Technology for Materials Synthesis and Processing, Wuhan University of Technology, Wuhan 430070, People's Republic of China; Department of Materials Science and Engineering, National University of Singapore, Singapore 117574, Singapore*

Yongkang An − *State Key Laboratory of Advanced Technology for Materials Synthesis and Processing, Wuhan University of Technology, Wuhan 430070, People's Republic of China*

Lu Wu − *State Key Laboratory of Advanced Technology for Materials Synthesis and Processing, Wuhan University of Technology, Wuhan 430070, People's Republic of China*

Jianguo Sun − *Department of Materials Science and Engineering, National University of Singapore, Singapore 117574, Singapore*

Fangyu Xiong − *State Key Laboratory of Advanced Technology for Materials Synthesis and Processing, Wuhan University of Technology, Wuhan 430070, People's Republic of China*

Han Tang − *State Key Laboratory of Advanced Technology for Materials Synthesis and Processing, Wuhan University of Technology, Wuhan 430070, People's Republic of China*

Shulin Chen − *State Key Laboratory of Advanced Technology for Materials Synthesis and Processing, Wuhan University of Technology, Wuhan 430070, People's Republic of China*

https://doi.org/10.1021/acsnano.2c09317
ACS Nano 2023, 17, 552−560

Yue Guo − *Department of Materials Science and Engineering, National University of Singapore, Singapore 117574, Singapore*

Lei Zhang − *State Key Laboratory of Advanced Technology for Materials Synthesis and Processing, Wuhan University of Technology, Wuhan 430070, People's Republic of China*

Complete contact information is available at: https://pubs.acs.org/10.1021/acsnano.2c09317

Author Contributions

Y.L. and Y.A. contributed equally to this work. All authors discussed the data and commented on the manuscript. The project was supervised by Q.A. and L.M.

Notes

The authors declare no competing financial interest.

ACKNOWLEDGMENTS

This work was supported by the National Key Research and Development Program of China (2020YFA0715000), the National Natural Science Foundation of China (52127816, 52172231, 52172233, 51972259), the Natural Science Foundation of Hubei Province (2022CFA087), the Industrialization Project of Xiangyang Technology Transfer Center of the Wuhan University of Technology (WXCJ-20220017), the Fundamental Research Funds for the Central Universities (WUT: 2020III043GX, 2020III015GX), and the Foshan Xianhu Laboratory of the Advanced Energy Science and Technology Guangdong Laboratory (XHT2020-003). Y.L. acknowledges the support of the China Scholarship Council (CSC) (No. 202106950024).

REFERENCES

(1) Ha, S.; Lee, K. T. Batteries: Converting to long stability. *Nat. Energy* **2016**, *1*, 16057.

(2) Wang, X.; Zhang, Z.; Xi, B.; Chen, W.; Jia, Y.; Feng, J.; Xiong, S. Advances and Perspectives of Cathode Storage Chemistry in Aqueous Zinc-Ion Batteries. *ACS Nano* **2021**, *15*, 9244−9272.

(3) Kundu, D.; Adams, B. D.; Duffort, V.; Vajargah, S. H.; Nazar, L. F. A high-capacity and long-life aqueous rechargeable zinc battery using a metal oxide intercalation cathode. *Nat. Energy* **2016**, *1*, 16119.

(4) Ma, L.; Schroeder, M. A.; Borodin, O.; Pollard, T. P.; Ding, M. S.; Wang, C.; Xu, K. Realizing high zinc reversibility in rechargeable batteries. *Nat. Energy* **2020**, *5*, 743−749.

(5) Han, M. M.; Huang, J. W.; Wu, X. W.; Liang, S. Q.; Zhou, J. Electrolyte Modulation Strategies for Rechargeable Zn Batteries. *Chin. J. Inorg. Chem.* **2022**, *38*, 1451−1469.

(6) Liu, Z.; Huang, Y.; Huang, Y.; Yang, Q.; Li, X.; Huang, Z.; Zhi, C. Voltage issue of aqueous rechargeable metal-ion batteries. *Chem. Soc. Rev.* **2020**, *49*, 180−232.

(7) Liu, Y.; Huang, M.; Xiong, F.; Zhu, J.; An, Q. Improved zinc-ion storage performance of the metal-free organic anode by the effect of binder. *Chem. Eng. J.* **2022**, *428*, 131092.

(8) Chen, X.; Ruan, P.; Wu, X.; Liang, S.; Zhou, J. Crystal Structures, Reaction Mechanisms, and Optimization Strategies of MnO_2 Cathode for Aqueous Rechargeable Zinc Batteries. *Acta Phys. -Chim. Sin.* **2021**, *0*, 2111003.

(9) Li, X.; Chen, Z.; Yang, Y.; Liang, S.; Lu, B.; Zhou, J. The phosphate cathodes for aqueous zinc-ion batteries. *Inorg. Chem. Front.* **2022**, *9*, 3986−3998.

(10) Blanc, L. E.; Kundu, D.; Nazar, L. F. Scientific Challenges for the Implementation of Zn-Ion Batteries. *Joule* **2020**, *4*, 771−799.

(11) Wang, T.; Li, C.; Xie, X.; Lu, B.; He, Z.; Liang, S.; Zhou, J. Anode Materials for Aqueous Zinc Ion Batteries: Mechanisms, Properties, and Perspectives. *ACS Nano* **2020**, *14*, 16321−16347.

(12) Zheng, J.; Zhao, Q.; Tang, T.; Yin, J.; Quilty, C. D.; Renderos, G. D.; Liu, X.; Deng, Y.; Wang, L.; Bock, D. C.; Jaye, C.; Zhang, D.; Takeuchi, E. S.; Takeuchi, K. J.; Marschilok, A. C.; Archer, L. A. Reversible epitaxial electrodeposition of metals in battery anodes. *Science* **2019**, *366*, 645−648.

(13) Ma, L.; Li, Q.; Ying, Y.; Ma, F.; Chen, S.; Li, Y.; Huang, H.; Zhi, C. Toward Practical High-Areal-Capacity Aqueous Zinc-Metal Batteries: Quantifying Hydrogen Evolution and a Solid-Ion Conductor for Stable Zinc Anodes. *Adv. Mater.* **2021**, *33*, 2007406.

(14) Cao, L.; Li, D.; Hu, E.; Xu, J.; Deng, T.; Ma, L.; Wang, Y.; Yang, X. Q.; Wang, C. Solvation Structure Design for Aqueous Zn Metal Batteries. *J. Am. Chem. Soc.* **2020**, *142*, 21404−21409.

(15) Han, M.; Yao, J.; Huang, J.; Tang, Y.; Wu, X.; Lu, B.; Zhou, J. Synergistic chemical and electrochemical strategy for high-performance Zn//MnO_2 batteries. *Chin. Chem. Lett.* **2022**, DOI: 10.1016/j.cclet.2022.05.007.

(16) Wang, Y.; Guo, T.; Yin, J.; Tian, Z.; Ma, Y.; Liu, Z.; Zhu, Y.; Alshareef, H. N. Controlled Deposition of Zinc-Metal Anodes via Selectively Polarized Ferroelectric Polymers. *Adv. Mater.* **2022**, *34*, 2106937.

(17) Yan, H.; Li, S.; Nan, Y.; Yang, S.; Li, B. Ultrafast Zinc−Ion−Conductor Interface toward High-Rate and Stable Zinc Metal Batteries. *Adv. Energy Mater.* **2021**, *11*, 2100186.

(18) Kang, L.; Cui, M.; Jiang, F.; Gao, Y.; Luo, H.; Liu, J.; Liang, W.; Zhi, C. Nanoporous $CaCO_3$ Coatings Enabled Uniform Zn Stripping/Plating for Long-Life Zinc Rechargeable Aqueous Batteries. *Adv. Energy Mater.* **2018**, *8*, 1801090.

(19) Zhang, P.-F.; Wu, Z.; Zhang, S.-J.; Liu, L.-Y.; Tian, Y.; Dou, Y.; Lin, Z.; Zhang, S. Tannin acid induced anticorrosive film toward stable Zn-ion batteries. *Nano Energy* **2022**, *102*, 107721.

(20) Shi, W.; Song, Z.; Wang, J.; Li, Q.; An, Q. Phytic acid conversion film interfacial engineering for stabilizing zinc metal anode. *Chem. Eng. J.* **2022**, *446*, 137295.

(21) Deng, C.; Xie, X.; Han, J.; Lu, B.; Liang, S.; Zhou, J. Stabilization of Zn Metal Anode through Surface Reconstruction of a Cerium-Based Conversion Film. *Adv. Funct. Mater.* **2021**, *31*, 2103227.

(22) Liu, Y.; Wang, J.; Sun, J.; Xiong, F.; Liu, Q.; An, Y.; Shen, L.; Wang, J.; An, Q.; Mai, L. A glutamate anion boosted zinc anode for deep cycling aqueous zinc ion batteries. *J. Mater. Chem. A* **2022**, *10*, 25029−25038.

(23) Wang, D.; Lv, D.; Liu, H.; Zhang, S.; Wang, C.; Wang, C.; Yang, J.; Qian, Y. In Situ Formation of Nitrogen-Rich Solid Electrolyte Interphase and Simultaneous Regulating Solvation Structures for Advanced Zn Metal Batteries. *Angew. Chem., Int. Ed.* **2022**, *61*, e202212839.

(24) Tang, Z.; Wang, H.; Wu, P. F.; Zhou, S. Y.; Huang, Y. C.; Zhang, R.; Sun, D.; Tang, Y. G.; Wang, H. Y. Electrode-Electrolyte Interfacial Chemistry Modulation for Ultra-High Rate Sodium-Ion Batteries. *Angew. Chem., Int. Ed.* **2022**, *61*, e202200475.

(25) Rudolph, W. W.; Brooker, M. H.; Tremaine, P. R. Raman Spectroscopy of Aqueous ZnSO4 Solutions under Hydrothermal Conditions: Solubility, Hydrolysis, and Sulfate Ion Pairing. *J. Solution Chem.* **1999**, *28*, 621−630.

(26) Yang, H.; Chang, Z.; Qiao, Y.; Deng, H.; Mu, X.; He, P.; Zhou, H. Constructing a Super-Saturated Electrolyte Front Surface for Stable Rechargeable Aqueous Zinc Batteries. *Angew. Chem., Int. Ed.* **2020**, *59*, 9377−9381.

(27) Hayes, A. C.; Kruus, P.; Adams, W. A. Raman spectroscopic study of aqueous $(NH_4)_2SO_4$ and $ZnSO_4$ solutions. *J. Solution Chem.* **1984**, *13*, 61−75.

(28) Qiu, M.; Sun, P.; Qin, A.; Cui, G.; Mai, W. Metal-coordination chemistry guiding preferred crystallographic orientation for reversible zinc anode. *Energy Storage Mater.* **2022**, *49*, 463−470.

(29) Gore, R. C.; Barnes, R. B.; Petersen, E. Infrared Absorption of Aqueous Solutions of Organic Acids and Their Salts. *Anal. Chem.* **1949**, *21*, 382−386.

(30) Sun, P.; Ma, L.; Zhou, W.; Qiu, M.; Wang, Z.; Chao, D.; Mai, W. Simultaneous Regulation on Solvation Shell and Electrode

Interface for Dendrite-Free Zn Ion Batteries Achieved by a Low-Cost Glucose Additive. *Angew. Chem., Int. Ed.* **2021**, *60*, 18247−18255.
(31) Zhang, Q.; Ma, Y.; Lu, Y.; Li, L.; Wan, F.; Zhang, K.; Chen, J. Modulating electrolyte structure for ultralow temperature aqueous zinc batteries. *Nat. Commun.* **2020**, *11*, 4463.
(32) Miao, L.; Wang, R.; Di, S.; Qian, Z.; Zhang, L.; Xin, W.; Liu, M.; Zhu, Z.; Chu, S.; Du, Y.; Zhang, N. Aqueous Electrolytes with Hydrophobic Organic Cosolvents for Stabilizing Zinc Metal Anodes. *ACS Nano* **2022**, *16*, 9667−9678.
(33) Huang, C.; Zhao, X.; Liu, S.; Hao, Y.; Tang, Q.; Hu, A.; Liu, Z.; Chen, X. Stabilizing Zinc Anodes by Regulating the Electrical Double Layer with Saccharin Anions. *Adv. Mater.* **2021**, *33*, 2100445.
(34) Myers, M.; Khir, F. L. M.; Home, M. A.; Mennell, C.; Gillbanks, J.; Tadich, A.; Baker, M. V.; Nener, B. D.; Parish, G. XPS/NEXAFS spectroscopic and conductance studies of glycine on AlGaN/GaN transistor devices. *Appl. Surf. Sci.* **2018**, *435*, 23−30.
(35) Li, C.; Shyamsunder, A.; Hoane, A. G.; Long, D. M.; Kwok, C. Y.; Kotula, P. G.; Zavadil, K. R.; Gewirth, A. A.; Nazar, L. F. Highly reversible Zn anode with a practical areal capacity enabled by a sustainable electrolyte and superacid interfacial chemistry. *Joule* **2022**, *6*, 1103−1120.
(36) An, Y.; Tian, Y.; Liu, C.; Xiong, S.; Feng, J.; Qian, Y. Rational Design of Sulfur-Doped Three-Dimensional $Ti_3C_2T_x$ MXene/ZnS Heterostructure as Multifunctional Protective Layer for Dendrite-Free Zinc-Ion Batteries. *ACS Nano* **2021**, *15*, 15259−15273.
(37) Hao, J.; Li, B.; Li, X.; Zeng, X.; Zhang, S.; Yang, F.; Liu, S.; Li, D.; Wu, C.; Guo, Z. An In-Depth Study of Zn Metal Surface Chemistry for Advanced Aqueous Zn-Ion Batteries. *Adv. Mater.* **2020**, *32*, 2003021.
(38) Zeng, X.; Mao, J.; Hao, J.; Liu, J.; Liu, S.; Wang, Z.; Wang, Y.; Zhang, S.; Zheng, T.; Liu, J.; Rao, P.; Guo, Z. Electrolyte Design for In Situ Construction of Highly Zn^{2+} -Conductive Solid Electrolyte Interphase to Enable High-Performance Aqueous Zn-Ion Batteries under Practical Conditions. *Adv. Mater.* **2021**, *33*, 2007416.
(39) Xie, X.; Liang, S.; Gao, J.; Guo, S.; Guo, J.; Wang, C.; Xu, G.; Wu, X.; Chen, G.; Zhou, J. Manipulating the ion-transfer kinetics and interface stability for high-performance zinc metal anodes. *Energy Environ. Sci.* **2020**, *13*, 503−510.
(40) Zheng, J.; Huang, Z.; Zeng, Y.; Liu, W.; Wei, B.; Qi, Z.; Wang, Z.; Xia, C.; Liang, H. Electrostatic Shielding Regulation of Magnetron Sputtered Al-Based Alloy Protective Coatings Enables Highly Reversible Zinc Anodes. *Nano Lett.* **2022**, *22*, 1017−1023.
(41) Hong, L.; Wu, X.; Wang, L. Y.; Zhong, M.; Zhang, P.; Jiang, L.; Huang, W.; Wang, Y.; Wang, K. X.; Chen, J. S. Highly Reversible Zinc Anode Enabled by a Cation-Exchange Coating with Zn-Ion Selective Channels. *ACS Nano* **2022**, *16*, 6906−6915.
(42) Liu, Q.; Chen, R.; Xu, L.; Liu, Y.; Dai, Y.; Huang, M.; Mai, L. Steric Molecular Combing Effect Enables Ultrafast Self-Healing Electrolyte in Quasi-Solid-State Zinc-Ion Batteries. *ACS Energy Lett.* **2022**, *7*, 2825−2832.
(43) Guo, Z.; Fan, L.; Zhao, C.; Chen, A.; Liu, N.; Zhang, Y.; Zhang, N. A Dynamic and Self-Adapting Interface Coating for Stable Zn-Metal Anodes. *Adv. Mater.* **2022**, *34*, 2105133.
(44) Cao, J.; Zhang, D.; Yue, Y.; Chanajaree, R.; Wang, S.; Han, J.; Zhang, X.; Qin, J.; Huang, Y. Regulating solvation structure to stabilize zinc anode by fastening the free water molecules with an inorganic colloidal electrolyte. *Nano Energy* **2022**, *93*, 106839.
(45) Zheng, J.; Cao, Z.; Ming, F.; Liang, H.; Qi, Z.; Liu, W.; Xia, C.; Chen, C.; Cavallo, L.; Wang, Z.; Alshareef, H. N. Preferred Orientation of TiN Coatings Enables Stable Zinc Anodes. *ACS Energy Lett.* **2022**, *7*, 197−203.

https://doi.org/10.1021/acsnano.2c09317
ACS Nano 2023, 17, 552−560